NOTES AND CORRESPONDENCE

The Riding Wave Removal Technique: Recent Developments

ERIC WERNER SCHULZ

Centre of Australian Weather and Climate Research, Australian Bureau of Meteorology, Melbourne, Victoria, Australia

(Manuscript received 31 January 2008, in final form 15 July 2008)

ABSTRACT

Recent advances in a technique to identify and catalog waves that ride on larger-scale carrier waves are described in detail. The latest developments allow the riding wave removal technique to correctly identify and replace riding waves at the Nyquist frequency scale. Examples of the technique are provided for two diverse datasets: the Black Sea and Lake George. A sample of the riding wave characteristics extracted using this method is presented.

1. Introduction

The role of small-scale waves in air–sea interaction has been explored in recent decades. At the microbreaker scale (wavelength around a few centimeters), their importance for wave breaking and the associated exchange of gases (e.g., Thorpe 1982; Keeling 1993), generation of marine aerosols (Bortkovskii 1987; Ling 1993), enhancement to momentum flux via breaking waves (Donelan 1990), and resultant mixing in the ocean (Rapp and Melville 1990) have been examined in field and laboratory experiments. The role of breaking waves in modifying the wave height spectrum has also been investigated by Manasseh et al. (2006).

The scale of breaking waves covers a large range from the microbreakers up to the dominant waves, and they are usually unevenly distributed in space and time. This heterogeneity is particularly prevalent in the microbreakers that ride on the dominant waves. Data analysis of these small-scale waves is not amenable to spectral methods, and manual identification has traditionally been used. Recent advances in data analysis techniques such as wavelet analysis (Liu and Babanin 2004), empirical mode decomposition (Huang et al. 1998), and the riding wave removal method (Banner et al. 2002) have allowed the characteristics of small-scale waves to be quantified. The development of technology capable of detecting breaking waves via acoustic (e.g., Farmer and Vagle 1988; Manasseh et al. 2006), radar (e.g., Jessup et al. 1990; Phillips et al. 2001), sonar (Thorpe 1992), infrared (Jessup et al. 1997), conductivity (Gemmrich and Farmer 1999; Lamarre and Melville 1992), and aerial imaging (Melville and Matusov 2002) has driven the need for more sophisticated wave counting methods.

Here we explore the riding wave removal (RWR) technique. The author was involved in developing the original RWR technique for Banner et al. (2002), which was subsequently used by Gemmrich and Farmer (2004). We provide the first detailed description of the RWR technique and include some recent advances. Demonstrations are given of the RWR technique applied to two diverse datasets, and subtleties of the method are discussed.

2. The technique

The RWR technique was developed to allow the small-scale waves riding on the backs of the larger-scale dominant wind waves to be identified and their characteristics cataloged. This enabled their role in wave breaking onset to be explored. The predecessor of the RWR technique is the traditional zero-crossing approach, such as that described by Gemmrich and Farmer (1999) where the local minima of the surface elevation are used to identify waves. In the presence of

Corresponding author address: Dr. Eric Schulz, Centre of Australian Weather and Climate Research, Australian Bureau of Meteorology, GPO Box 1289, Melbourne, VIC 3001, Australia.
E-mail: e.schulz@bom.gov.au

DOI: 10.1175/2008JTECHO621.1

riding waves, the zero-crossing methods underestimate the presence of larger-scale waves as they are effectively subdivided into shorter waves. As a result, the overall bias can be significant and is unpredictable. The RWR technique extends the zero-crossing method by progressively identifying and replacing the riding waves iteratively from the shortest to the longest scales, with the local maxima and minima recalculated after each scale iteration, thus reducing any bias. We stress that the technique is designed to detect the presence and catalog the characteristics of riding waves, not to filter out riding waves from the underlying carrier waves. The term ‘‘removal’’ refers to the process step of replacing the detected riding waves with a synthesized segment that matches the underlying wave. This process step allows for riding waves on multiple scales to be detected and cataloged.

The RWR technique is generally applied to point measurement time series datasets. These datasets do not contain directional information. This is a limitation of the observation that clearly sets limits on the insight the RWR technique can yield. Any user of the RWR technique needs to be aware of these limitations. The RWR technique has been designed to primarily identify and count riding waves. At this level the technique is useful for determining the presence or absence of riding waves. The calculation of higher-order riding wave characteristics such as height, period, and steepness may be biased by assumptions such as a unidirectional wave field.

a. Riding wave replacement segment

The critical part of the technique is the construction of the segment that replaces the riding wave, as the introduction of spurious noise, or changes to the energy of larger-scale waves is undesirable. Banner et al. (2002) constructed a replacement segment based on a cubic polynomial fitted to six points. The points were selected as three successive points on both sides of the riding wave, the closest beginning at the slope extrema. A schematic of a carrier wave and two riding waves, and the constructed replacement segment is displayed in Fig. 1. The riding wave on the left face of the carrier wave is at the Nyquist frequency scale, while the riding wave on the right face is at a larger scale.

Since then, the RWR technique has undergone two main developments. First, the construction of the replacement segment has been refined with the aim of generating a smoother result and minimizing energy ‘‘leakage’’ to other wave scales. Second, the RWR technique has been extended so that it can properly identify and replace riding waves at the Nyquist frequency scale.

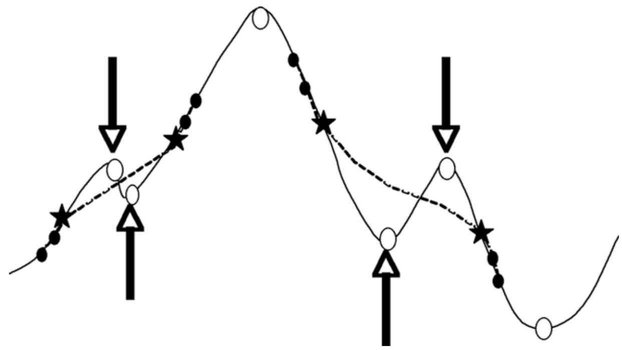

FIG. 1. Schematic of a carrier wave and associated riding waves. The replacement segments are calculated as described in Banner et al. (2002). The solid line represents surface elevation. Open circles indicate local maxima and minima, stars are slope extrema, and closed circles are other significant points also used to construct the replacement segment (dashed line). In this example the other significant points are the first and second points adjacent to the slope extrema on the outside of the identified riding wave. The arrows indicate the identified riding wave. The riding wave characteristics are determined solely by the maxima and minima indicated by the arrow, not the replacement segment.

For any riding wave with frequency below the Nyquist, a replacement segment is constructed from a fourth-order polynomial least squares, fitted to the crest and trough immediately adjacent to the riding wave and a midpoint in the riding wave. Points used to fit the crest and trough are the local maxima or minima and the adjacent point farther away from the riding wave. The additional point representing the midpoint of the riding wave is included in the fit to encourage the replacement segment to pass through the middle of the riding wave, thereby minimizing any change to the energy of the underlying carrier wave. Figure 2 displays an identical riding and carrier waves as in Fig. 1, but the replacement segments are constructed using the most recent advances to the RWR technique. Once again, the riding wave on the left face of the carrier wave is at the Nyquist frequency scale, while the riding wave on the right face is at a larger scale.

For riding waves at the Nyquist frequency, the replacement segment is linear and fitted to a point immediately before and after the riding wave crest and trough. This avoids any overlap of the replacement segment onto adjacent data, which becomes critical when riding waves at the Nyquist frequency occur in groups.

The original and modified RWR technique depicted in Figs. 1 and 2 will extract identical riding wave characteristics in this instant. The difference in technique effects how the underlying carrier wave is modified when the riding wave is replaced. This may affect the characteristics of larger-scale riding waves that are subsequently detected.

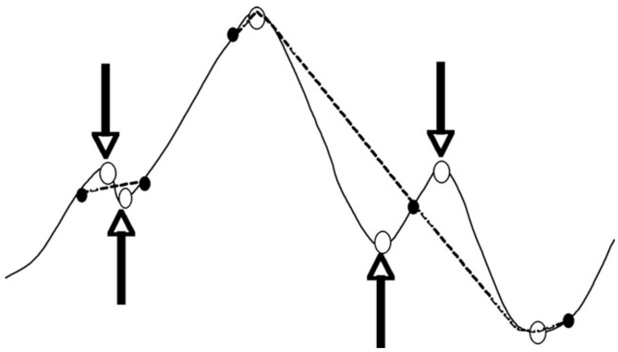

FIG. 2. As in Fig. 1, but the replacement segment is calculated by the new method. In this example the other significant points are the point at either side of the riding wave trough and crest if it is at the Nyquist frequency. For lower frequencies, the other significant points are the point adjacent to the next nearest local maxima and minima, and a point between the riding wave crest and trough.

b. *Riding wave removal sequence*

The RWR technique is an iterative procedure that detects, characterizes, and removes riding waves in a surface elevation signal. The RWR is achieved by identifying all the shortest riding waves present in the signal, and replacing them with a smooth segment. The technique is then repeated for the next shortest riding waves, and so on until all riding waves down to some arbitrary scale have been detected and removed.

The sequence of processing steps is as follows:

1) Determine the peak frequency using spectral methods.
2) Locate all local maxima and minima.
3) Rank the waves by length according to distance between adjacent maxima and minima.
4) Select all the shortest waves that are greater than those previously processed (to avoid counting any processing generated smaller-scale waves). Ignore waves with a height less than a threshold value. The initial pass looks for waves at the Nyquist frequency scale.
5) Record information about each riding wave, including wavelength or period, height, steepness, position on the forward/rear face of the carrier wave, and position in the time series.
6) Take each selected wave in turn and construct and insert the replacement segment, working from one end of the data record to the other. The constructed segment is linear if the riding wave is at the Nyquist frequency; otherwise, it is fourth-order polynomial.
7) Exit if the technique has removed waves down to the desired cutoff frequency scale; otherwise, return to step 2 with the reconstructed signal.

Banner et al. (2002) empirically determined a cutoff scale of 1.9 times the peak frequency, which maximized the number of counted wave crests in the dominant wave band. The period (wavelength) of the riding wave is defined as twice the distance between adjacent maxima and minima in the time (space) domain. Here we have selected a wave height threshold of 1×10^{-4} m, as elevation variations less than this are induced by the RWR processing. Banner et al. (2002) selected a threshold of 0.1 m. The threshold should be based on the limits of accuracy of the observing instrument. For the purpose of demonstrating the RWR technique, we assume there are no observational errors.

Figure 3 depicts the procedure used to replace two adjacent Nyquist frequency scale riding waves. Figure 3a depicts the two riding waves and part of the carrier wave, with thin vertical lines identifying data points. The first riding wave on the left, which can be identified by the two leftmost open circles (for the peak and trough) is replaced first by fitting a linear replacement segment (dashed line) to the points (closed circles) adjacent to the peak and trough. We note that the point immediately adjacent to the right of the riding wave is also the crest of the adjacent riding wave. Figure 3b depicts the modified carrier wave, the second riding wave, and the next replacement segment (dashed line). The peak and trough of the second riding wave is once again identified by open circles and points used in the fit by closed circles. Figure 3c depicts the modified carrier wave with both riding waves replaced. A subtlety of this technique is that while the location of riding waves is determined only once at the beginning of each pass at a given scale, the sequential replacement of riding waves does modify the elevation of the carrier and riding wave signal. A clear example can be seen at the third data point in Fig. 3. We note that the original RWR method is not capable of correctly removing riding waves in this situation. First, because it is difficult to determine slope maxima when adjacent points are part of a similar scale riding wave. Second, the replacement segment would overlap onto adjacent riding waves, not only making the polynomial fitting difficult, but creating discontinuities when subsequent riding waves are removed and elevation modifications impinge on adjacent riding waves.

3. Results

a. *Synthetic test cases*

An initial set of tests was conducted to increase confidence that the RWR technique was performing the riding wave count as expected. A series of three synthetic signals were tested. An underlying sinusoid car-

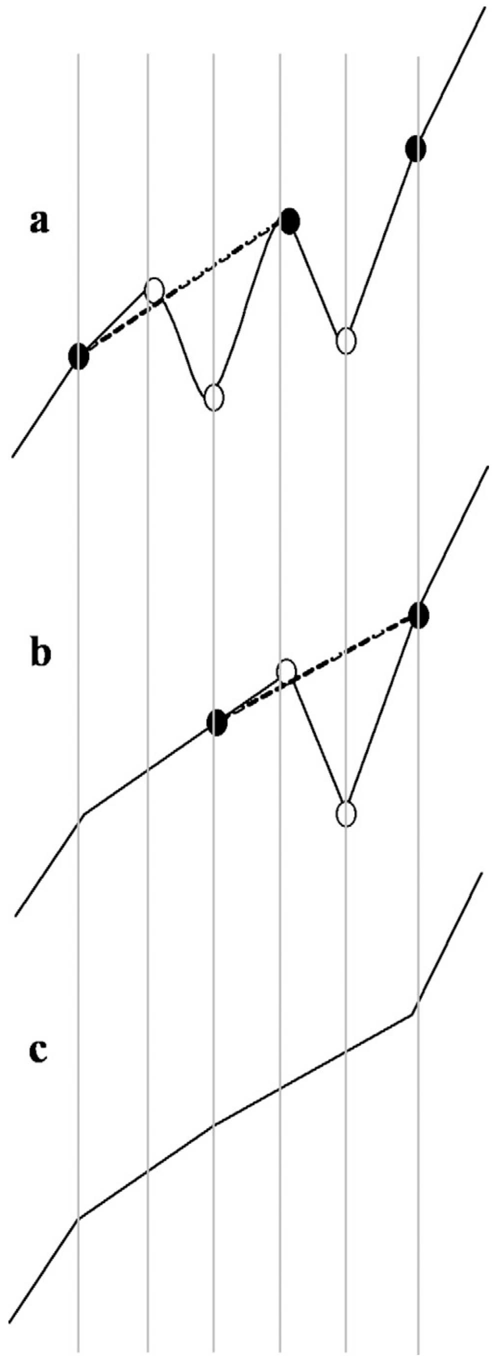

FIG. 3. (a) Idealized group of two adjacent riding waves at the Nyquist frequency scale, where the local maxima and minima (open circles) and adjacent points (closed circles) are identified, and a linear replacement segment is applied to the riding wave on the left. Faint vertical lines are provided to assist visualizing the RWR process. (b) How the segment for the riding wave on the right is generated using the updated value of what was the trough of the old riding wave on the left. (c) The final elevation with the two riding waves removed.

rier wave (frequency = 0.1 Hz, amplitude = 10, time series length = 1000 s) was constructed. The first synthetic signal simply had sinusoid riding waves (frequency = 1 Hz, amplitude = 2) uniformly and continuously superimposed on the carrier wave. This resulted in the synthesis of 1000 riding waves, while the RWR technique counted 901 riding waves. With a pi/6 phase shift the count increased to 919. The second test involved randomly removing complete riding waves from the first synthetic signal, yielding a pseudorandom set of riding waves, although all in phase with each other and the carrier wave. In this case the RWR technique overestimated the number of riding waves by around 15%. It is not trivial to determine the number of synthesized riding waves in this test as a 1-Hz riding wave may be counted as two riding waves depending on the phase difference between the carrier and riding wave. The third test involved synthesizing a signal very similar to that depicted in Fig. 1 (two riding waves per carrier wave) and keeping the carrier wave unchanged as before. In this case the RWR technique correctly counted all 200 riding waves. The RWR technique performs as designed and counts riding waves to within approximately 10% of the expected number based on synthetic test cases.

b. Field observation dataset examples

We provide examples of the RWR technique applied to two datasets collected during different field campaigns: Lake George (Young et al. 2005) and the Black Sea (Babanin and Soloviev 1998).

The first example comes from Lake George, which is a shallow lake (0.2–2-m depth) in New South Wales, Australia. Wave staffs were deployed to allow observations of fetch-limited (approximately 1–10 km) finite-depth waves outside of the surf zone, representative of intermediate-depth wind seas. The first example is a 6-min dataset sampled every 0.04 s. Mean 10-m wind speed is approximately 20 m s^{-1} and the waves have a peak period of 2.6 s, and significant wave height of 0.45 m.

Figure 4 displays an example of the RWR technique applied to the observational time series from the Lake George experiment. The displayed time series is 125 samples (5 s) long with a cutoff period for the riding wave replacement (at 1.9 times peak frequency of the full time series) of 1.4 s. Figure 4a shows the observed signal, and Fig. 4b includes the reconstructed signal after the first pass when riding waves at the Nyquist frequency have been removed. A number of riding waves of this scale have been removed (at sample positions: 4855, 4890, 4905, 4914, 4920, 4942, 4954, 4959, and 4967) and replaced with linear segments. The next three

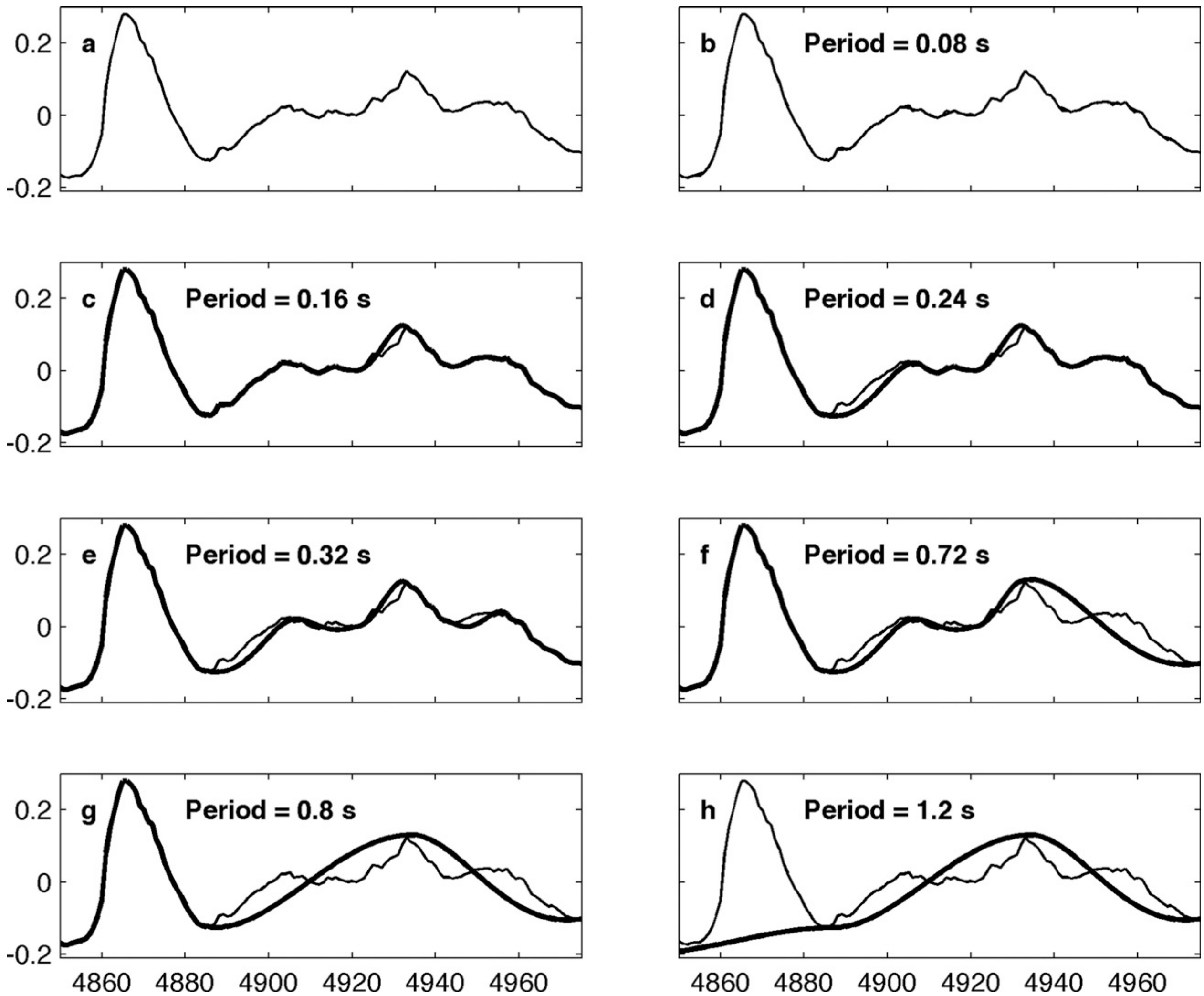

FIG. 4. Lake George surface elevation (5-s sample). The original (thin line) and reconstructed (thick line) time series are displayed. (a) Original time series, (b) with Nyquist period 0.08-s riding waves removed, and passes (c) 2, (d) 3, (e) 4, (f) 9, (g) 10, and (h) 15 corresponding to their respective riding wave periods at 0.16, 0.24, 0.32, 0.72, 0.8, and 1.2 s. [Note that only thin lines are used in (b) to assist with figure interpretation.]

passes remove riding waves at periods of 0.16 (Fig. 4c), 0.24 (Fig. 4d), and 0.32 s (Fig. 4e). The fifth pass does not alter the time series in the selected sample, but the ninth and tenth passes (Figs. 4f,g) remove riding waves at periods 0.72 and 0.8 s. Subsequent passes do not alter the time series in the selected sample, until pass 15 (Fig. 4h) at period 1.2 s. Pass 14 is at a period of 1.12 s (not displayed). In this particular case it would appear that 1.9 times the peak frequency is probably too low for the cutoff frequency, as it causes large changes to the original signal. A cutoff frequency of 0.89 Hz (1.12 s), which equates to 2.3 times the peak frequency, would be more suitable.

The second example comes from the Black Sea, which is a large inland sea (400 km × 1200 km) with depths typically greater than 1000 m. Observations were obtained from wind-wave recorders on an oil platform situated in 30-m-deep waters ideal for observing deep-water waves. This example is a 6-min dataset sampled every 0.05 s. Mean 10-m wind speed is 9.5 m s^{-1} and the waves have a peak frequency of 0.22 Hz, and significant wave height of 1.1 m.

A similar analysis is performed for a short 35-s segment of the Black Sea example (Fig. 5). The display period spans 700 samples, with a cutoff period (at 1.9 times peak frequency of the full time series) of 2.4 s. Figure 5a shows the observed signal, and subsequent panels display the original and reconstructed surface elevation after passes 4 (period removed at 0.4 s), 5 (0.5 s), 6 (0.6 s), 8 (0.8 s), 12 (1.2 s), 17 (1.7 s), and 21 (2.3 s).

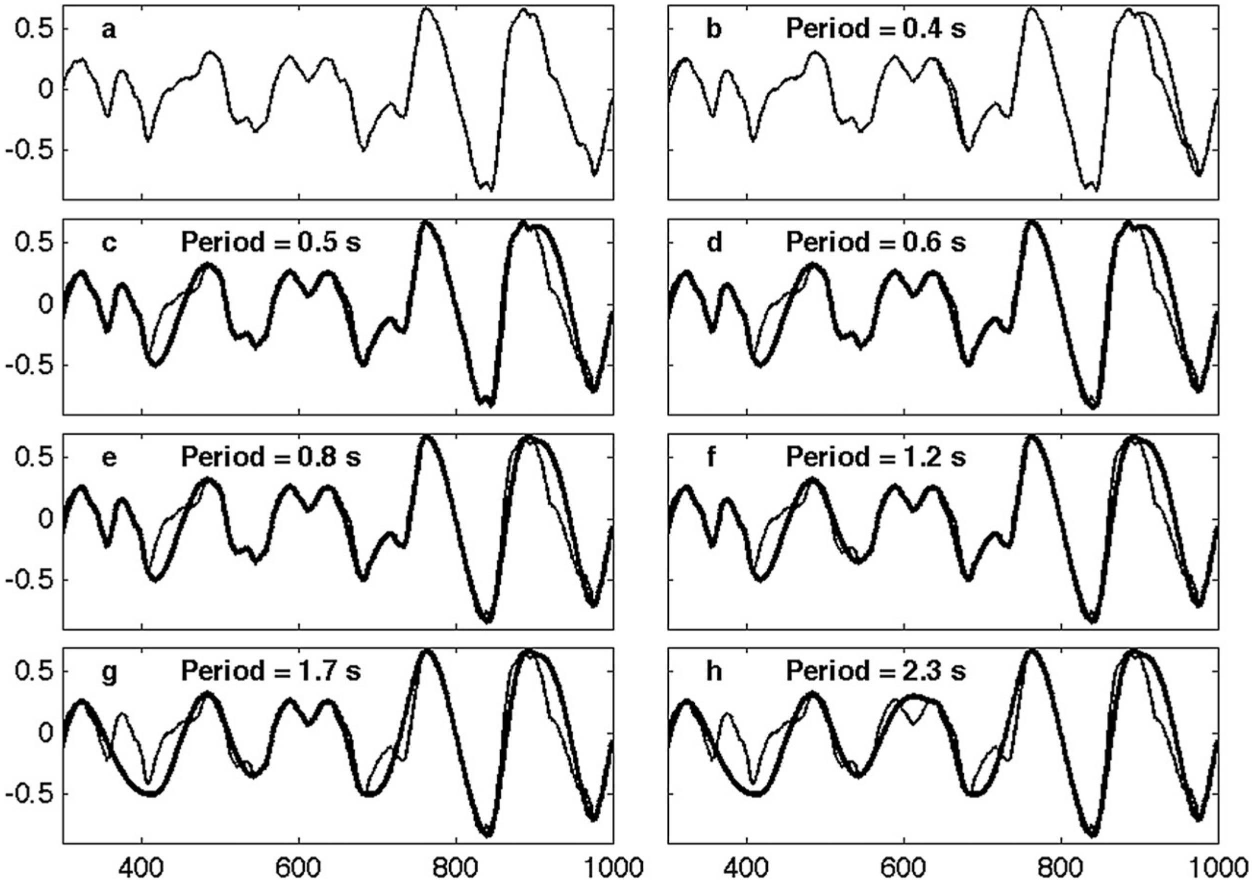

FIG. 5. Black Sea surface elevation (35-s sample). The original (thin line) and reconstructed (thick line) time series are displayed. (a) Original time series, (b) modified time series with 0.4-s period riding waves removed, and passes (c) 5, (d) 6, (e) 8, (f) 12, (g) 17, and (h) 21 corresponding to their respective riding wave periods at 0.5, 0.6, 0.8, 1.2, 1.7, and 2.3 s.

We also perform a test on the Lake George data to check that the energy contained in the identified riding waves matches the change in energy from the original elevation time series, and the post-RWR processed time series. This is achieved by calculating the mean square of the time derivative of the original surface elevation ($h0$), $E_{h0} = \langle (dh0/dt)^2 \rangle = 0.155$, and the signal after riding wave removal (h), $E_h = \langle (dh/dt)^2 \rangle = 0.119$. The decomposed riding wave energy is calculated from the mean of the squares of amplitude x radian frequency: $E_{\mathrm{rw}} = \langle (A\ x\ \omega)^2 \rangle = 0.08$. For an analytic solution (sinusoid) the ratio between the mean square time derivative of elevation and mean square amplitude x radian frequency is 2 (i.e., E_{h0} and E_h are multiplied by 2 yielding $E_{h0} = 0.31$ and $E_h = 0.238$). The calculation of E_{rw} diverges from the analytical solution when the wave is nonlinear, which is almost certainly the case for riding waves. In addition, the time series cannot fully resolve the high-frequency waves, which may lead to some very large derivatives. Despite the above-mentioned issues, the riding wave energy ($E_{\mathrm{rw}} = 0.08$) is comparable to the difference between the high-frequency energy of the original and processed signal ($E_{h0} - E_h = 0.072$).

4. Discussion

The objective of the RWR technique is to identify and record information about riding waves. The scope of the information recorded is briefly mentioned in section 2b. A fundamental measurement is the presence and, hence, position of the riding wave in the dataset to allow correlations of occurrence of riding waves and wave breaking to be achieved. The number of occurrences, wave height, and steepness of riding waves at a particular scale are also of interest. The occurrence (panel a), wave height (panel b), and steepness (panel c) for the Lake George (Fig. 6) and Black Sea (Fig. 7) examples are displayed. The wave height (H) is calculated as the change in elevation between trough and crest. The wave steepness is calculated as $H/L = 2\pi H/(gT^2)$, where T is the wave period and the linear deep-water dispersion relationship is used.

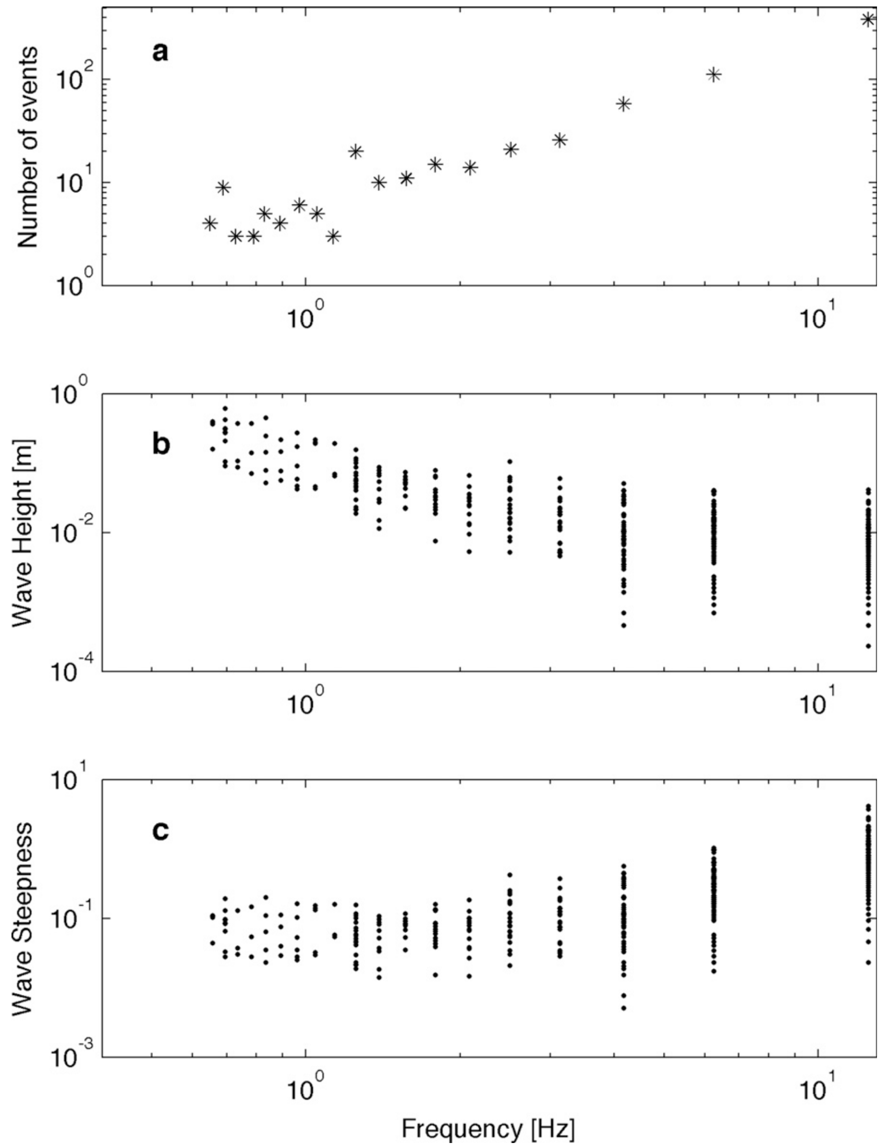

FIG. 6. Riding wave statistics for Lake George. (a) Number of riding wave events, (b) wave height, and (c) steepness vs frequency (riding wave scale).

The Lake George and Black Sea examples exhibit some common features. Increased occurrence and steepness, and smaller wave heights are evident as the scale of the riding waves decreases. There is no flattening off in the number of counts as the Nyquist frequency scales are approached. There are also a significant number of riding waves at the Nyquist frequency with wave heights comparable to those at the lower frequency scales. The wave steepness exceeds the theoretical stokes limit (i.e., 0.14) at times. This occurs more often as the Nyquist frequency is approached. This may indicate that a despiking or smoothing preprocessing step is required for these datasets.

Wave steepness is calculated by calculating wave length from frequency via the dispersion relationship. The frequency may undergo a Doppler shift—particularly for riding waves on the crest of much larger-scale carrier waves that can have significant large orbital velocities relative to the riding wave phase speed. The relative Doppler shift can be estimated.

In presence of a current u, for a wave with frequency ω_0, the single-point measured frequency is $\omega = \omega_0 + ku$, where k is the wavenumber. Hence, $\omega = \omega_0 + (\omega_0^2/g)u$. When the orbital velocity is concurrent with (opposite to) the wave propagation, the single-point measured frequency is greater (less) than ω_0. For symmetric and

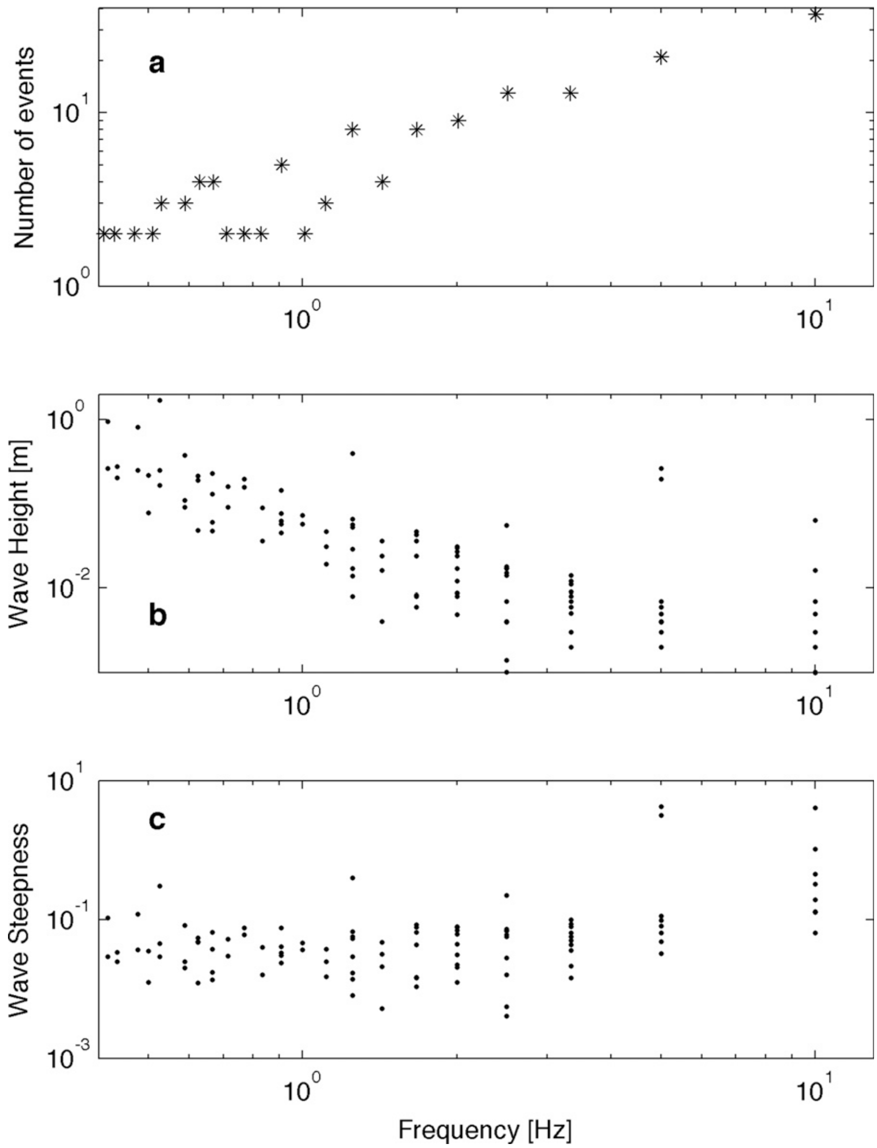

FIG. 7. As in Fig. 6, but for the Black Sea.

nonskewed waves the mean orbital velocity over the wave period is zero, and therefore the mean single-point measured frequency is measured correctly, but the mean spectral estimate at that frequency is shifted, assuming an even distribution of riding waves along the phase of the carrier wave.

If we assume the linear theory that crest orbital velocity is proportional to its height (H) at a given frequency (Ω), $u = \Omega x H/2$, then we can derive the maximum Doppler shift for a given frequency. For Lake George (Black Sea) the maximum wave heights are around 0.6 m (1.5 m), with a period of 3.5 s (5 s), yielding an orbital velocity of 0.54 m s^{-1} (0.94 m s^{-1}). For a riding wave at $\omega = 1$ Hz, $\omega_0 = 0.79$ Hz (0.70 Hz); that is, a 27% (43%) change. These estimations are for the largest few waves in the time series. The standard deviation of surface elevation for Lake George (Black Sea) is 0.11 m (0.28 m), 18% (19%) of the maximum value. Assuming a linear dependence, the Doppler shift is reduced to 5% (8%) of the frequency. This effect is for the wave crests only. If we assume that the crest region persists for 10% of the phase length of the wave, the effect can be divided by 10, yielding a final Doppler shift of 0.5% (0.8%). Even for a riding wave near the Nyquist frequency, the Doppler shift errors are only around 5%.

It is evident that there is a much lower density of riding waves in the Black Sea example compared to

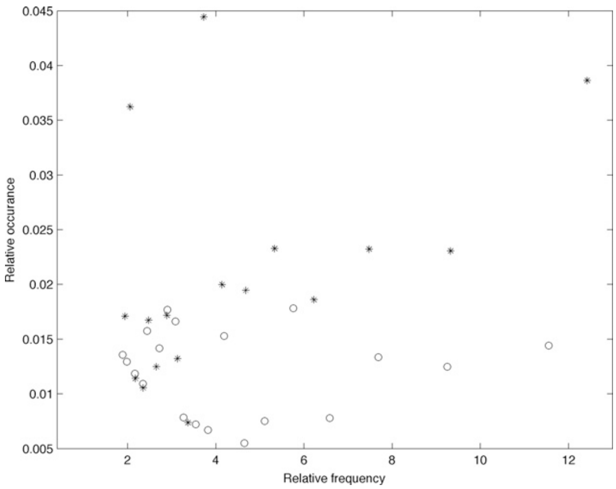

FIG. 8. Relative occurrence vs relative frequency, where relative occurrence is occurrence divided by $f \times T$ (where f is frequency of the riding wave and T the length of the time series in seconds), and relative frequency is frequency of the riding wave divided by peak frequency of the original time series. Data are displayed for Lake George (*) and the Black Sea (o).

Lake George. The Black Sea data has approximately one-quarter the number of riding waves; for example, at the 5-Hz scale, the RWR technique counts 20 riding waves for the Black Sea, and approximately 80 for Lake George. The same riding wave occurrence is presented in another way in Fig. 8 with relative occurrence versus relative frequency. Relative occurrence is defined as occurrence divided by maximum possible occurrence (where the maximum is the frequency in hertz multiplied by the record length in seconds). Relative frequency is the frequency divided by peak frequency. For relative frequencies greater than about 3.5 times the peak frequency, the Lake George data displays higher relative occurrence. This may be due to the different experimental conditions where the Black Sea data are for deep-water conditions, while the Lake George data are for finite-depth conditions.

The RWR technique is built on the assumption that there is a dominant ''carrier'' wave on which the riding wave is superimposed. At the smaller scales, the riding wave is replaced with a synthesized segment that is merged into the larger-scale waves. As the dominant frequency is approached, the RWR technique starts to break down and generate nonphysical solutions as it attempts to remove waves that are clearly ''nonriding waves.'' This can be seen in the example of the Lake George data displayed in Fig. 5h, where the large peak on the left, which does not appear to be a riding wave, is removed at the period scale of 1.2 s. This would suggest that a more conservative cutoff frequency in the range 2–2.5 times the peak frequency should be applied, particularly when a broad dominant frequency is present, rather than the 1.9 times the peak frequency previously suggested by Banner et al. (2002).

There is some choice in the selection of the order of the polynomial fit used in the replacement segment. Tests have show that increasing the order from third to fourth reduces the generation of small-scale waves or noise, and also allows the RWR technique to approach closer to the dominant frequency before generating nonphysical solutions. Higher-order polynomial fits require a greater number of points for the fit to be unique.

The RWR technique is designed to identify and record information about riding waves. Its usefulness for low-pass filtering is limited as there is some tendency for distortion of waves at the dominant and larger scales with small changes to the location of peaks and troughs, skewing of the waveform, and exaggeration of the amplitude.

In summary, recent advances in the RWR technique have allowed for a more correct treatment of riding waves at the Nyquist frequency scale. This has increased the scope of the technique for high-frequency applications and will allow further understanding to be gained in small-scale riding waves.

Acknowledgments. I would like to acknowledge Alexander Babanin and Richard Manasseh, whose research needs have encouraged the further development of the RWR technique. The many useful comments from the anonymous reviewers improved the description of the RWR technique.

REFERENCES

Babanin, A. V., and Yu. P. Soloviev, 1998: Field investigation of transformation of the wind wave frequency spectrum with fetch and the stage of development. *J. Phys. Oceanogr.,* **28,** 563–576.

Banner, M. L., J. R. Gemmrich, and D. M. Farmer, 2002: Multiscale measurements of ocean wave breaking probability. *J. Phys. Oceanogr.,* **32,** 3364–3375.

Bortkovskii, R. S., 1987: *Air-Sea, Exchange of Heat and Moisture during Storms.* D. Reidel, 194 pp.

Donelan, M. A., 1990: Air-sea interaction. *The Sea*, B. LeMehaute and D. M. Hanes, Eds., Ocean Engineering Science, Vol. 9, John Wiley and Sons, 239–292.

Farmer, D. M., and S. Vagle, 1988: On the determination of breaking surface wave distribution. *J. Geophys. Res.,* **93C,** 3591–3600.

Gemmrich, J. R., and D. M. Farmer, 1999: Observations of the scale and occurrence of breaking surface waves. *J. Phys. Oceanogr.,* **29,** 2595–2606.

——, and ——, 2004: Near-surface turbulence in the presence of breaking waves. *J. Phys. Oceanogr.,* **34,** 1067–1086.

Huang, N. E., and Coauthors, 1998: The empirical mode decomposition and the Hilbert spectrum for nonlinear and nonstationary time series analysis. *Proc. Roy. Soc. London,* **454A,** 903–955.

Jessup, A. T., W. C. Keller, and W. K. Melville, 1990: Measurements of sea spikes in microwave backscatter at moderate incidence. *J. Geophys. Res.,* **95,** 9679–9688.

——, C. J. Zappa, M. R. Loewen, and V. Hesany, 1997: Infrared remote sensing of breaking waves. *Nature,* **385,** 52–55.

Keeling, R. F., 1993: On the role of large bubbles in air-sea gas exchange and supersaturation in the ocean. *J. Mar. Res.,* **51,** 237–271.

Lamarre, E., and W. K. Melville, 1992: Instrumentation for measurement of void-fraction in breaking waves: Laboratory and field results. *IEEE J. Oceanic Eng.,* **17,** 204–215.

Ling, C. S., 1993: Effect of breaking waves on the transport of heat and vapor fluxes from the ocean. *J. Phys. Oceanogr.,* **23,** 2306–2372.

Liu, P. C., and A. V. Babanin, 2004: Using wavelet spectrum analysis to resolve breaking events in the wind wave time series. *Ann. Geophys.,* **22,** 3335–3345.

Manasseh, R., A. Babanin, C. Forbes, K. Rickards, I. Bobevski, and A. Ooi, 2006: Passive acoustic determination of wave-breaking events and their severity across the spectrum. *J. Atmos. Oceanic Technol.,* **23,** 599–618.

Melville, W. K., and P. Matusov, 2002: Distribution of breaking waves at the ocean surface. *Nature,* **417,** 58–63.

Phillips, O. M., E. L. Posner, and J. P. Hansen, 2001: High range resolution radar measurements of the speed distribution of breaking events in wind-generated ocean waves: Surface impulse and wave energy dissipation rates. *J. Phys. Oceanogr.,* **31,** 450–460.

Rapp, R. J., and W. K. Melville, 1990: Laboratory measurements of deep-water breaking waves. *Philos. Trans. Roy. Soc. London,* **331A,** 731–800.

Thorpe, S. A., 1982: On the clouds of bubbles formed by breaking wind-waves in deep water, and their role in air-sea gas transfer. *Philos. Trans. Roy. Soc. London,* **304A,** 155–210.

——, 1992: Bubble clouds and the dynamics of the upper ocean. *Quart. J. Roy. Meteor. Soc.,* **118,** 1–22.

Young, I. R., M. L. Banner, M. A. Donelan, A. V. Babanin, W. K. Melville, F. Veron, and C. McCormick, 2005: An integrated system for the study of wind wave source terms in finite depth water. *J. Atmos. Oceanic Technol.,* **22,** 814–828.